Delft University of Technology

MALDI TIMS IMS of Disialoganglioside Isomers GD1a and GD1b in Murine Brain Tissue

Djambazova, Katerina V.; Dufresne, Martin; Migas, Lukasz G.; Kruse, Angela R.S.; Van De Plas, Raf; Caprioli, Richard M.; Spraggins, Jeffrey M.

Important note
To cite this publication, please use the final published version (if applicable).
Please check the document version above.

MALDI TIMS IMS of Disialoganglioside Isomers—GD1a and GD1b in Murine Brain Tissue

Katerina V. Djambazova, Martin Dufresne, Lukasz G. Migas, Angela R. S. Kruse, Raf Van de Plas, Richard M. Caprioli, and Jeffrey M. Spraggins*

Cite This: *Anal. Chem.* 2023, 95, 1176−1183

Read Online

ACCESS | ıll Metrics & More | 📰 Article Recommendations | 🆂🅸 Supporting Information

ABSTRACT: Gangliosides are acidic glycosphingolipids, containing ceramide moieties and oligosaccharide chains with one or more sialic acid residue(s) and are highly diverse isomeric structures with distinct biological roles. Matrix-assisted laser desorption/ionization imaging mass spectrometry (MALDI IMS) enables the untargeted spatial analysis of gangliosides, among other biomolecules, directly from tissue sections. Integrating trapped ion mobility spectrometry with MALDI IMS allows for the analysis of isomeric lipid structures in situ. Here, we demonstrate the gas-phase separation and identification of disialoganglioside isomers GD1a and GD1b that differ in the position of a sialic acid residue, in multiple samples, including a standard mixture of both isomers, a biological extract, and directly from thin tissue sections. The unique spatial distributions of GD1a/b (d36:1) and GD1a/b (d38:1) isomers were determined in rat hippocampus and spinal cord tissue sections, demonstrating the ability to structurally characterize and spatially map gangliosides based on both the carbohydrate chain and ceramide moieties.
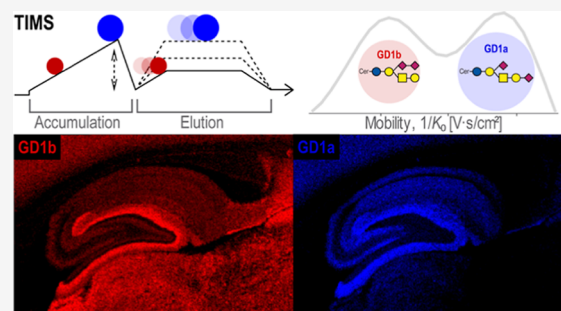
Gangliosides are acidic glycosphingolipids that are highly abundant in the mammalian nervous system.[1,2] As critical components of neuronal and glial cells, they play an essential role in neuronal development and maturation, as well as cellular signalling.[3,4] These molecules have been implicated in brain injury,[5] neurological diseases including Guillain-Barre syndrome,[6,7] Alzheimer's disease,[8] and Huntington's disease[9,10] and remain an active area of interest for developing therapeutics.

Gangliosides consist of a hydrophobic ceramide lipid backbone and an oligosaccharide chain of varying length with one or more sialic acid residues (Figure S1).[2] The major mammalian brain gangliosides share the same tetrasaccharide core and have multiple sialylation sites, giving rise to many possible isomeric forms. For example, GM1, GD1a, GD1b, and GT1b share the same tetrasaccharide core and make up over 80% of the entire mammalian ganglioside content.[11] GD1a and GD1b differ in the position of a single sialic acid residue: GD1a has a sialic acid on both the internal and terminal galactose units, and GD1b has both sialic acids attached to the internal galactose residue (Figure S2).

Generally, ganglioside distributions have been characterized in situ using immunohistochemistry (IHC) approaches. These techniques provide carbohydrate epitope information but can cross react with glycoproteins carrying similar sugar chains.[12,13] Furthermore, a drawback of IHC is that it provides no information on the ceramide backbone composition. The complete analysis of gangliosides in their native form is crucial in understanding their roles in different physiological

processes.[11,13,14] Mass spectrometry (MS) has been a critical tool for the detection and characterization of gangliosides because of its high molecular specificity and sensitivity.[15] MS analysis of gangliosides is known to cause extensive precursor ion fragmentation, which poses a challenge for both identification and quantitation of intact gangliosides. Because of this, softer ionization sources that reduce the degree of in-source fragmentation, such as electrospray ionization (ESI) and matrix-assisted laser desorption/ionization (MALDI),[16,17] have been preferred for ganglioside analysis.[11,17] MALDI imaging mass spectrometry (IMS) enables highly specific mass analysis while retaining analyte spatial information.[18] In a typical MALDI IMS experiment, thin sections of tissues are mounted on a conductive glass slide and coated with a UV-absorbing matrix. A laser raster of this sample produces an individual mass spectrum at each laser ablation position, and molecular images are generated by plotting the ion intensity as a heat map across all the ablation spots (pixels) sampled.[19] MALDI IMS has previously been employed to map the localization of gangliosides within biological tissues, including murine and human central nervous system tissues.[16,20−23]

However, obtaining comprehensive structural information remains a significant challenge without the use of additional techniques.[21−26]

Liquid chromatography (LC), ion fragmentation (MS[n]), and ion mobility separations can be integrated with MALDI IMS to address the structural complexity of gangliosides.[27] Although highly informative, MS[n] and LC techniques are often highly targeted and/or require lengthy acquisition times. Alternatively, ion mobility enables gas-phase separation of molecules according to their shape, size, and charge on timescales (μs−ms) compatible with typical MALDI IMS throughputs. Ion mobility separation techniques include drift tube ion mobility spectrometry,[28,29] traveling wave ion mobility spectrometry (TWIMS),[30,31] structures for lossless ion manipulations (SLIM),[32,33] field asymmetric ion mobility spectrometry,[34−36] and trapped ion mobility spectrometry (TIMS).[37,38] Each of these technologies, with the exception of SLIM, have been coupled to MALDI IMS.[39,40]

TWIMS MS has been used for in-depth analysis of gangliosides. Clemmer and coworkers have used ESI TWIMS MS for comprehensive untargeted analysis of human brain gangliosides.[41−43] In the context of structural characterization of ganglioside isomers, Ekroos and coworkers recently demonstrated the separation of isomers GD1a(d36:1) and GD1b(d36:1) using a prototype SLIM MS instrument.[44] The isomeric gangliosides were resolved both in a 1:1 mixture, as well as in a wild-type hemi-brain mouse brain extract.[44] Jackson et al. demonstrated the combination of ion mobility and MALDI for the analysis of GD1a and GD1b, where they show higher drift times for the GD1a isomer.[25] Woods and coworkers have reported the distributions of GD1(d36:1) after a water-loss (m/z 1817.95), to provide some insights into the possible spatial localizations of GD1b. This was possible as GD1b more readily undergoes water loss than GD1a.[45] However, the spatial distributions of a- and b-ganglioside isomers have not been directly demonstrated in a MALDI imaging context.

Here, we demonstrate the capability of MALDI TIMS IMS to differentiate ganglioside isomers GD1a and GD1b in tissue. Briefly, TIMS utilizes an electric field gradient (EFG) applied to an ion tunnel to trap and separate ions through opposing forces from the carrier gas and electric field. For analysis, the EFG is gradually reduced to sequentially elute ions with ascending mobilities.[37,46] Previous MALDI TIMS IMS experiments have demonstrated the utility of the platform for enhanced sensitivity and specificity of lipids in imaging experiments, as well as the separation/localization of isobaric and some isomeric phospholipids in situ.[38,46−51]

We distinguish GD1a and GD1b using a 1:1 standard mixture, a total ganglioside extract from tissue, and directly from an intact thin tissue section with MALDI TIMS IMS. The unique spatial distributions of GD1a/b(d36:1) and GD1a/b(d38:1) were mapped in both rat brain and spinal cord samples at 20 μm spatial resolution.

■ METHODS

Materials. 2′,5′-dihydroxyacetophenone (DHA), ammonium sulfate, and anti-GD1a ganglioside antibody were purchased from Sigma-Aldrich (St. Louis, MO, USA). High-performance liquid chromatography-grade acetonitrile, methanol, ethanol, and chloroform were purchased from Fisher Scientific (Pittsburgh, PA, USA). Ganglioside extracts were purchased from Avanti Polar Lipids (Alabaster, AL, USA),

control rat brain was purchased from BioIVT (Westbury, NY, USA), and control rat spinal cord was purchased from Pel-Freeze Biologicals (Rogers, AZ, USA). Goat anti-mouse IgG secondary antibody conjugated to Alexa Fluor Plus 647 was purchased from Invitrogen (Waltham, MA, USA), and DAPI fluoromount-G mounting media was purchased from SouthernBiotech (Birmingham, AL, USA).

Sample Preparation. Control rat brain and spinal cord were cryosectioned to 10 μm thickness using a CM3050 S cryostat (Leica Biosystems, Wetzlar, Germany) and thaw-mounted onto conductive indium tin oxide-coated glass slides (Delta Technologies, Loveland, CO, USA). Matrix deposition protocols were based on a published procedure:[23] 2′,5′-DHA with 62.5 μM ammonium sulfate in 60% ethanol−water was sprayed for a final matrix density of 1.23 μg/mm^2. The matrix was applied using a robotic sprayer—M5 Sprayer equipped with a sample heating tray (HTX Technologies, LLC, Chapel Hill, NC, USA). Specific spraying conditions are listed in Table S1. GD1a and GD1b ganglioside extracts (powder) were dissolved in chloroform, aliquoted in vials, dried down with nitrogen gas, and re-dissolved in 80% methanol for a final extract concentration of 2 mg/mL. The total porcine brain ganglioside extract had a final concentration of 10 mg/mL. The mixtures were spotted on indium tin oxide-coated glass slides and sprayed with the matrix.

Matrix-Assisted Laser Desorption/Ionization Trapped Ion Mobility Spectrometry Mass Spectrometry. All experiments were carried out on a prototype MALDI timsTOF Pro mass spectrometer (Bruker Daltonics, Bremen, Germany).[49] The $1/K_0$ range, EFG scan time and rate, m/z range, and other specific imaging parameters are listed in Tables S2 and S3. For standard analysis, data were acquired at 20 μm spatial resolution with ∼80% laser power at 10 kHz, 200 shots per pixel, and ∼300 pixels per sample. MALDI TIMS IMS specific data are listed in Tables S2 and S3.

Histology, Microscopy, and Tissue Annotation. Following the IMS experiments, the matrix was removed from the samples using 100% ethanol (10 s) and rehydrated with 70% ethanol (10 s). Tissues were stained using a modified cresyl violet stain (Table S4).[52] Brightfield microscopy of stained tissues was obtained using a Zeiss AxioScan Z1 slide scanner (Carl Zeiss Microscopy GmbH, Oberkochen, Germany). Annotations of anatomical regions were made on histologically stained tissue sections with the help of *The Allen Mouse Brain Atlas*,[53,54] *The Rat Brain in Stereotaxic Coordinates*,[55] and *The Atlas of Rat Spinal Cord*.[56]

Immunofluorescence. Immunofluorescence (IF) was performed to verify the localization of GD1a in the rat brain and spinal cord tissue sections. Serial tissue sections were fixed with 4% paraformaldehyde in phosphate-buffered saline (PBS) for 10 min, followed by blocking in PBS containing 1% bovine serum albumin and 0.5% Tween 20. The sections were hybridized with monoclonal anti-GD1a ganglioside antibody (1:50 dilution, Sigma-Aldrich MAB5606Z) in PBS containing 1% bovine serum albumin and 0.5% Tween 20 for 16 h. Antibody binding was detected using goat anti-mouse IgG secondary antibody conjugated to Alexa Fluor Plus 647 (1:500 dilution, Thermo Fisher A32728) for 1 h. Tissue sections unexposed to primary antibody were used to determine the level of non-specific secondary antibody binding. Sections were mounted with DAPI fluoromount-G mounting media (Southern Biotech) prior to fluorescent imaging. Microscopy was

collected using a Zeiss AxioScan Z1 with DAPI and Cy5 channels (Figures S3 and S4).

Identifications and Data Processing. Serial tissue sections were analyzed for further structural investigation. To eliminate the possibility of isobaric interference, a tissue section was analyzed using ultrahigh-spectra resolution FT ICR MS (resolving power $\sim$ 200,000 at m/z 1544) (Figure S5). MALDI TIMS MS/MS was used to show diagnostic and preferential a- and b-series fragments from standards (Figure S6) and to confirm ganglioside identification from serial tissue section (Figure S7). MALDI TIMS IMS data were analyzed using DataAnalysis (Bruker Daltonics) and visualized using SCiLS (Bruker Daltonics) and custom in-house developed software. Hotspot removal was applied in SCiLS to normalize each signal intensity to the maximum intensity detected for a given ion. This allows the color map to be extended, enhancing perception of the texture and dynamic range.

■ RESULTS AND DISCUSSION

MALDI TIMS Analysis of GD1a/GD1b Isomer from Extracts. Ganglioside extracts were analyzed under two different conditions: high TIMS resolving power (scan rate < 0.01 V/ms, with a 1100 ms t_{ramp} time) and moderate TIMS resolving power (scan rate—0.03 V/ms, with a 550 ms t_{ramp} time) (Table S2). Isomeric GD1a and GD1b were first analyzed individually to determine their respective mobilities under MALDI TIMS conditions. The two major GD1 species observed in both GD1a and GD1b standards have ceramide backbones of d36:1 and d38:1. Both species were detected as $[\mathrm{M-H}]^-$, $[\mathrm{M-CO_2-H}]^-$, $[\mathrm{M-H_2O-H}]^-$, and $[\mathrm{M+Na-2H}]^-$ adducts (Figure S8). The deprotonated forms of GD1a/b(d36:1) and GD1a/b(d38:1), detected at m/z 1835.96 and m/z 1863.99 respectively, were analyzed to investigate the ability to separate GD1 isomers. Under the high TIMS resolving power conditions, the individual $1/K_0$-values of the deprotonated species GD1b(d36:1) and GD1a(d36:1) were determined to be 2.12 and 2.13 V s/cm^2, respectively (Figure 1A). From the extracted ion mobilogram of the mixture, a

partial separation of the two isomers was observed. Using the same TIMS conditions, GD1b(d38:1) and GD1a(d38:1) isomers were partially resolved in a 1:1 mixture with $1/K_0$ values of 2.14 and 2.15 V s/cm^2, respectively (Figure 1B). Additionally, we analyzed a total ganglioside extract demonstrating the partial separation of GD1a/b for both (d36:1) and (d38:1) species (Figure S9). As these data were acquired with the goal of maximizing the TIMS resolving power, the experiment was repeated to show a separation that was more amenable to a MALDI IMS throughput (550 ms t_{ramp} time, $\sim$600 ms/pixel) (Figure S10). Our findings indicate that GD1b and GD1a isomers can be partially resolved in a 1:1 mixture of standards and in a total ganglioside extract, where the b-series isomers have more compact structures leading to lower $1/K_0$ values. These findings are consistent with previous MALDI-ion mobility experiments by Jackson et al.[25] and SLIM MS experiments by Ekroos and coworkers.[44]

MALDI TIMS IMS Separation and Localization of GD1a/GD1b in Rat Brain and Spinal Cord Tissue. *Rat Brain Tissue.* GD1a and GD1b species are the most abundant ganglioside species in the mammalian brain.[45] Both a- and b-series disialogangliosides have distinct localizations within the brain, previously characterized using IHC. MALDI TIMS IMS data were collected from a sagittal rat brain section (left hemisphere, lateral value $\sim$ 0.8−0.9 mm), at 20 μm spatial resolution. The average mass spectrum shows that the mass range from $\sim m/z$ 1800 to 1900 was dominated by the GD1(d36:1) and GD1(d38:1) species, detected as $[\mathrm{M-H}]^-$, $[\mathrm{M-CO_2-H}]^-$, $[\mathrm{M-H_2O-H}]^-$, and $[\mathrm{M+Na-2H}]^-$ adducts (Figure S11). A cresyl violet stain was used to highlight the regions of interest in the hippocampus that were analyzed by MALDI IMS (Figure 2A). Ion images of m/z 1835.96 (purple) and m/z 1863.99 (green) show the unique distributions of GD1(d36:1) and GD1(d38:1), respectively (Figure 2B). Comparing the ion images with the annotated stain, we observed that GD1(d36:1) was more pronounced in the granular layer of the dentate gyrus, the pyramidal layer of the CA3 and CA2 regions, and along the fiber tracks. GD1(d38:1), on the other hand, was more pronounced in the molecular layer of the dentate gyrus, in the midbrain, and along the edges of the subiculum. The overlaid ion images represent a composite image of a- and b-series isomers for both d36:1 and d38:1. Further investigation using the TIMS dimension reveled two partially resolved peaks for m/z 1835.96, corresponding to deprotonated GD1a(d36:1) and GD1b(d36:1). Individual standards, GD1a and GD1b, were also acquired using the same conditions to aid in identification (Figure S12). Ion images of each ion mobility peak of m/z 1835.96 (Figure 3A) show the unique spatial distributions of both a-(blue) and b-(red) series isomers. GD1a and GD1b were expressed in all layers of the hippocampus but differed in their relative intensities in specific subregions. We observed that the a-isomer was more pronounced in the granular layer of the dentate gyrus, while the b-isomer was more abundant in the subiculum, as well as the midbrain, and thalamus, where the signal from the a-series was noticeably absent. The extracted ion mobilogram of m/z 1863.99 highlighted two partially resolved ions, corresponding to a- and b-series GD1(d38:1) (Figure 3B). Although the two ions were not as well resolved in the gas phase, their localizations within the rat brain tissues were different. The a-isomer was observed in the granular layer of the dentate gyrus and was more pronounced in the striatum radiata and striatum oriens of the CA3 region.
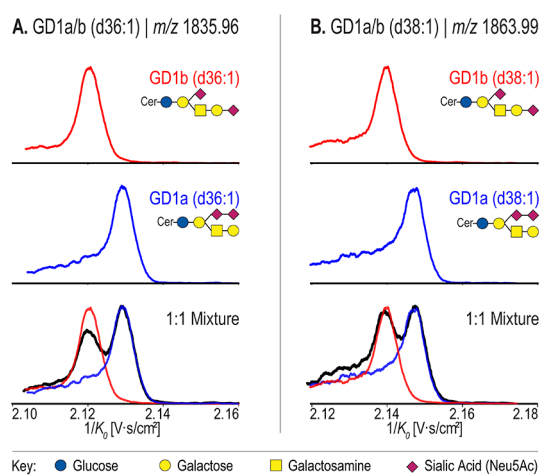

A. GD1a/b (d36:1) | m/z 1835.96   **B.** GD1a/b (d38:1) | m/z 1863.99

GD1b (d36:1)   GD1b (d38:1)

GD1a (d36:1)   GD1a (d38:1)

1:1 Mixture   1:1 Mixture

$1/K_0$ [V·s/cm^2] $1/K_0$ [V·s/cm^2]

Key: ● Glucose   ● Galactose   ■ Galactosamine   ◆ Sialic Acid (Neu5Ac)

Figure 1. MALDI TIMS ion mobilograms of deprotonated GD1a(d36:1) (blue) and GD1b(d36:1) (red) were separated in a 1:1 mixture of both standards (black) (A); deprotonated GD1a(d38:1) (blue) and GD1b(d38:1) (red) were separated in a 1:1 mixture of both (black) standards (B). Mobilograms were extracted from an average MALDI IMS data set, acquired in negative ion mode with a TIMS ramp time of 1100 ms.
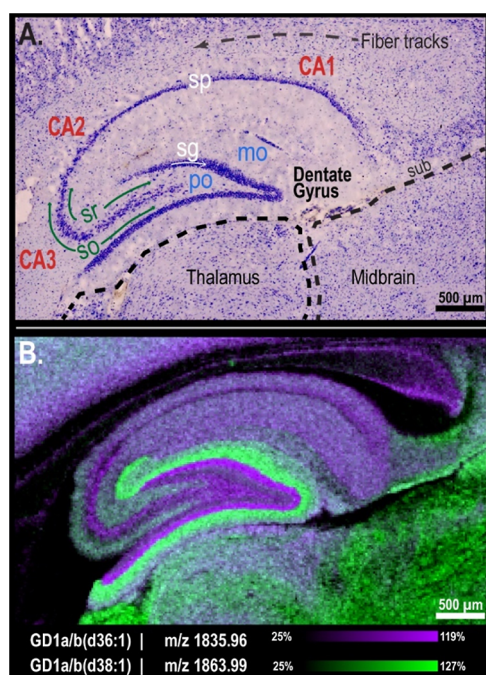
Figure 2. Cresyl violet stain of a sagittal rat brain section highlights features of interest in the hippocampus: Ammon's hors regions—CA1, CA2, and CA3 (in red), the dentate gyrus, the molecular layer (mo), polymorph layer (po), pyramidal layer (sp), granule cell layer (sg), stratum radiatum (sr), stratum oriens (so), and the subiculum (sub) (A). Overlaid ion images of m/z 1835.96 (purple) and m/z 1863.99 (green) show the different distribution of GD1(d36:1) and GD1(d38:1), respectively, where both distributions are composite a- and b-series gangliosides (B).

GD1b was also more pronounced in the granular layer of the CA1 and CA2 regions, where GD1a was below the limit of detection. GD1a was, however, present in the striatum radiata and the striatum oriens of CA1 and CA2. Similar to GD1a/b(d36:1), the most significant distinction between the two isomers was the detection of the a-series in the thalamus but not the midbrain or the subiculum. These GD1a-specific spatial distributions were also confirmed by IF, which was performed on a serial rat brain tissue section using a commercially available GD1a antibody (Figure S3). Our MALDI TIMS IMS findings were not only consistent with the IF data but also with previous IHC experiments of mouse and rat brains, showing GD1a and GD1b localizations,[13,57] and with previous IMS data.[23,24] Woods and co-workers had previously reported mapping of GD1b(d36:1) by imaging the water loss at m/z 1817.95, which is more preferential for the b-series gangliosides.[45] Similarly, using differences in the fragmentation pathways of GD1a and GD1b can be crucial in identifying the isomers (Figure S7) but may not be informative when trying to elucidate their unique spatial distributions. The two isomers have similar fragmentation pathways, where only GD1b produces a unique fragment ion—m/z 581, corresponding to the disialo fragment. This ion, however, has low abundance, making its distributions difficult to map in an MALDI MS/MS experiment.

Here, we highlight the subtle differences of GD1 subspecies that differ in both ceramide composition and sialic acid localizations. This work shows that with the combination of MALDI IMS and ion mobility separations, the spatial distributions of GD1a(d36:1), GD1b(d36:1), GD1a(d38:1), and GD1b(d38:1) and any combination of thereof can be visualized directly from thin tissue sections (Figure 4A−D). In addition to the two overlaid ion images in Figure 2, there are four additional ion overlay combinations possible, as high-lighted in Figure 4. As ganglioside role and function is influenced by the ceramide moieties and the carbohydrate chains, this level of structural specificity in an imaging context is important to further understand their role in biology and disease. These data were acquired with moderate TIMS resolving power, resulting in the partial separation of the isomeric gangliosides. Because of this, partial overlap in the ions' spatial distributions is possible. Higher TIMS resolutions can be achieved to better separate the two isomeric species; however, this comes at the expense of longer acquisition times,
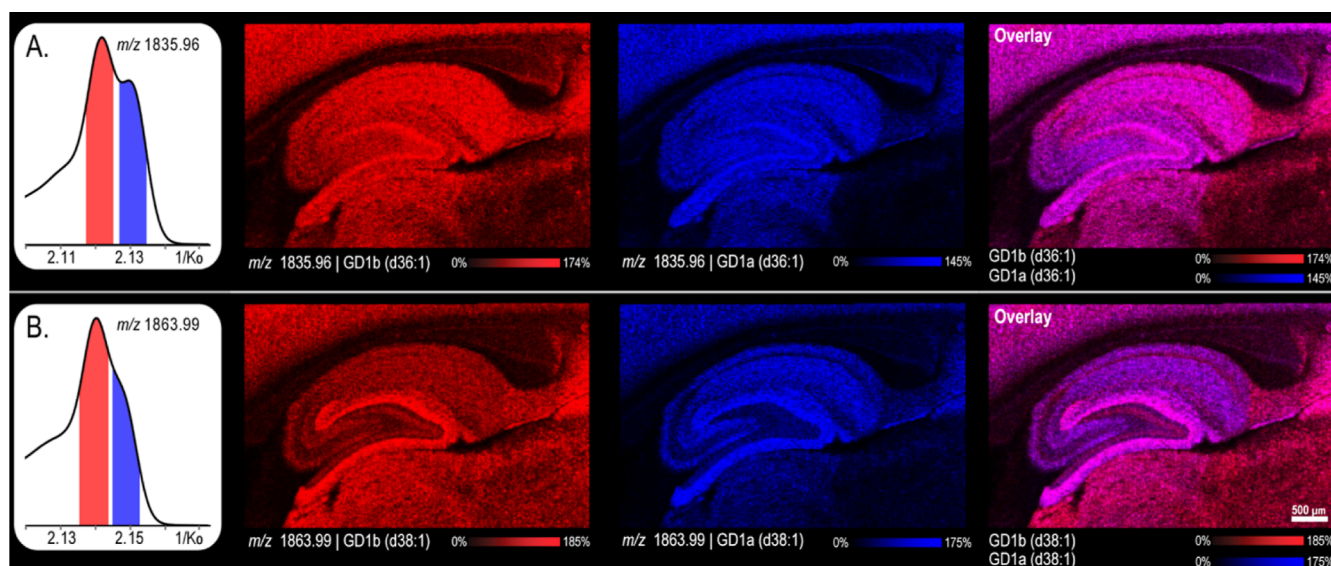

Figure 3. Extracted ion mobilograms of m/z 1835.96 (A) and m/z 1863.99 (B) demonstrate the partial separation of GD1b-(red) and GD1a (d36:1) (blue) in rat hippocampus tissue section. Ion images of GD1b (red), GD1a (blue) isomers, and an overlay of both ions can be seen for both GD1(d36:1) (A) and GD1(d38:1) (B).
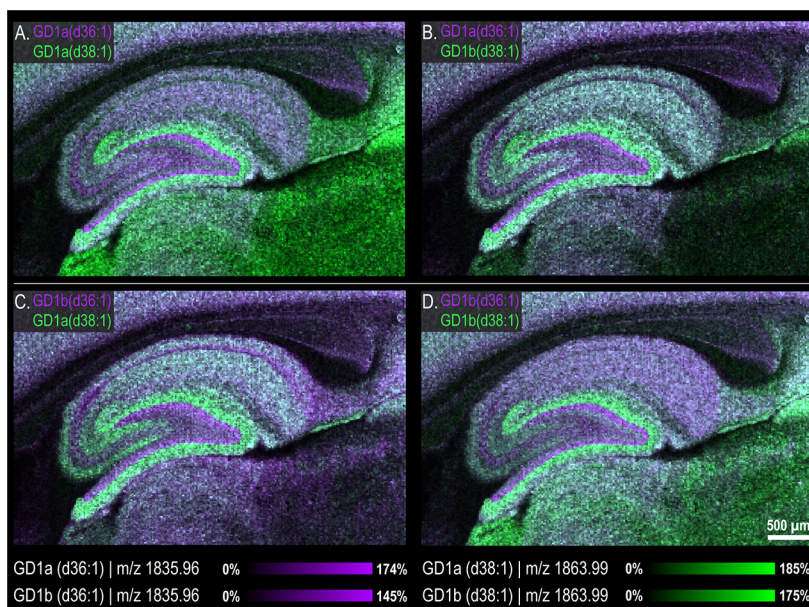
Figure 4. Overlay ion images of a and b-series isomers for GD1(d36:1) and GD1(d38:1): GD1a(d36:1) and GD1a(d38:1) (A), GD1a(d36:1) and GD1b (d38:1) (B), GD1b(d36:1) and GD1a(d38:1) (C), and GD1b(d36:1) and GD1b(d38:1) (D).
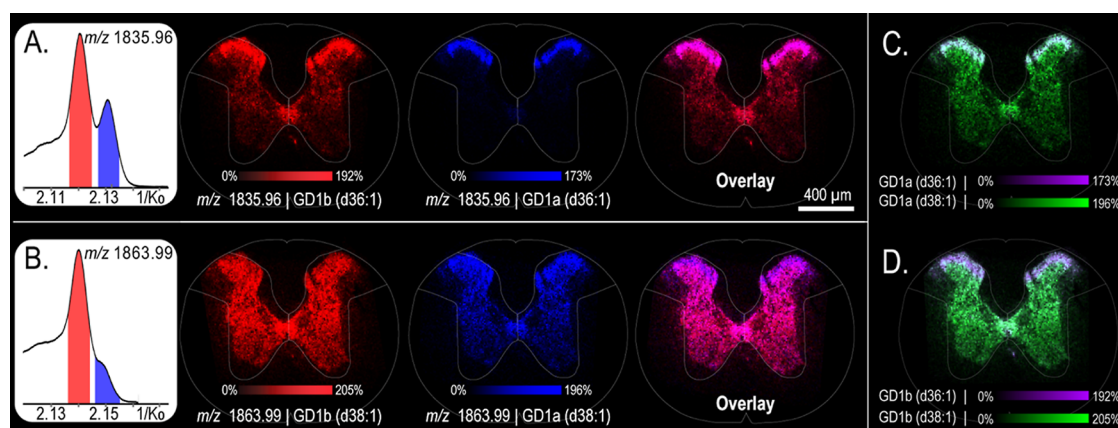

Figure 5. Extracted ion mobilograms of m/z 1835.96 (A) and m/z 1863.99 (B) demonstrate the partial separation of GD1b-(red) and GD1a (d36:1) (blue) in the rat spinal cord section. Ion images of GD1b (red), GD1a (blue) isomers, and an overlay of both ions can be seen for both GD1(d36:1) (A) and GD1(d38:1) (B). Overlay ion images of GD1a (d36:1) and (d38:1), as well as GD1b (d36:1) and (d38:1) are highlighted in (C,D), respectively.

which may not be suitable for all imaging applications. To illustrate the highest achievable GD1a/GD1b separation in this imaging experiment, longer ramp times were used to image smaller tissue sections, such as rat spinal cord tissue, in the following section.

Spinal Cord. To further investigate the unique distributions of GD1a and GD1b isomers in murine nervous tissue, rat spinal cord tissue was analyzed. A transverse section of the sympathetic intermediolateral horn (roughly T6−T11 region) was selected as the a- and b-series GD1 localizations have been previously highlighted in the literature by IHC.[13] A cresyl violet microscopy image was annotated to show the regions of interest (Figure S13). Considering the relatively small size of the tissue section, MALDI TIMS parameters were optimized to maximize the separations and demonstrate the highest resolution separation of GD1a/b isomers in situ. The extracted ion mobilograms of the GD1(d36:1) and GD1(d38:1) revealed two isomeric species (Figure 5A,B, respectively). From the ion images of m/z 1835.96 (Figure 5A), we can see

that the b-series was found throughout the gray matter with higher intensity in the rexed laminae 1 and 2 of the dorsal horn. The a-series isomer only present in the rexed laminae. The ion images of m/z 1863.99 (Figure 5B) revealed that GD1b was detected throughout the gray matter. The a-series isomer was more pronounced in the rexed laminae but could also be detected in the gray matter, specifically around the central canal (Figure 5B). An overlay of GD1b(d36:1) and GD1b(d38:1) (Figure 5C) revealed that the signal in the rexed laminae was mostly due to the d36:1, where the d38:1 was more pronounced in the gray matter. The overlay of GD1a(d36:1) and GD1a(d38:1) (Figure 5D) shows that GD1a(d36:1) was more intense in the laminae than the d38:1, which was detected throughout the gray matter.

The spatial distributions of the GD1a isomers were further confirmed by IF of GD1a (Figure S3), which shows a higher intensity of the GD1a isomer in the rexed laminae. Our findings are consistent with previous IHC studies that show GD1a and GD1b, and with MALDI IMS studies that show the

spatial distribution of GD1(d36:1) versus GD1(d38:1) localization within murine spinal cord tissue.[13] Neither of these previous approaches were able to resolve the nuanced differences in the ceramide composition and carbohydrate chain simultaneously. For example, the composite ion images of GD1a(d36:1) and GD1a(d38:1) (Figure 5C) could not be resolved with IF where the spatial distributions of GD1a are dictated by the 36:1 species. Similarly, mapping the localization of GD1a(d36:1) and GD1b(d38:1), as well as GD1b(d36:1) and GD1a(d38:1), could not be achieved with either MALDI IMS or IHC alone. These examples highlight the utility of MALDI TIMS IMS for the gas-phase separation of GD1a- and b-series isomers in situ.

CONCLUSIONS

This work demonstrates the capabilities of MALDI TIMS IMS in elucidating the spatial distribution of both GD1a/b(36:1) and GD1a/b(38:1) species in tissue samples that cannot be achieved through standard IHC experiments or typical MALDI IMS workflows. We demonstrated the unique spatial distribution of these gangliosides directly from rat brain and spinal cord tissues, using this MALDI TIMS IMS. Differentiating between these isomers is crucial in a biological context as the two species have different spatial distributions and are differentially impacted by diseases, such as Alzheimer's disease. For example, Taki et al.[58] previously demonstrated lower expression levels of polysialylated b-series gangliosides in the hippocampal gray matter of AD patients, where no significant alterations were revealed for a-series gangliosides. Furthermore, an increase in the ratio of GD1b with C20:0 fatty acyl chain to that containing C18:0 was identified as a cause of amyloid beta assembly in the precuneus of AD patients.[59] The ability to both structurally characterize and spatially map gangliosides with high specificity in situ will enable new biomedical studies that may reveal the role of this important class of molecules in health and disease.

ASSOCIATED CONTENT

Ⓢ Supporting Information

The Supporting Information is available free of charge at https://pubs.acs.org/doi/10.1021/acs.analchem.2c03939.

> Major brain ganglioside structure; GD1a and GD1b molecular structures; matrix deposition parameters; MALDI TIMS experimental parameters; MALDI IMS parameters; cresyl violet staining procedure; immunofluorescence—GD1a in the rat brain; immunofluorescence—GD1a in the rat spinal cord; MALDI FT-ICR data; fragmentation spectra of GD1a and GD1b standards; on-tissue fragmentation spectra of GD1-(d36:1) and GD1(d38:1); average mass spectrum of GD1a and GD1b extracts; extracted ion mobilograms from the total ganglioside extract; extracted ion mobilograms for ganglioside isomers with moderate TIMS resolving power; average mass spectrum of rat hippocampus; extracted ion mobilograms of GD1a/b standards and rat brain data; and rat spinal cord annotations (PDF)

AUTHOR INFORMATION

Corresponding Author

Jeffrey M. Spraggins − Department of Chemistry, Vanderbilt University, Nashville, Tennessee 37235, United States; Mass Spectrometry Research Center, Vanderbilt University, Nashville, Tennessee 37235, United States; Department of Biochemistry, Vanderbilt University, Nashville, Tennessee 37205, United States; Department of Cell and Developmental Biology, Vanderbilt University, Nashville, Tennessee 37232, United States; ⓞ orcid.org/0000-0001-9198-5498; Email: Jeff.Spraggins@vanderbilt.edu

Authors

Katerina V. Djambazova − Department of Chemistry, Vanderbilt University, Nashville, Tennessee 37235, United States; Mass Spectrometry Research Center, Vanderbilt University, Nashville, Tennessee 37235, United States; ⓞ orcid.org/0000-0002-2680-9014

Martin Dufresne − Mass Spectrometry Research Center, Vanderbilt University, Nashville, Tennessee 37235, United States; Department of Biochemistry, Vanderbilt University, Nashville, Tennessee 37205, United States; ⓞ orcid.org/0000-0002-1731-3666

Lukasz G. Migas − Delft Center for Systems and Control, Delft University of Technology, 2628 CD Delft, The Netherlands; ⓞ orcid.org/0000-0002-1884-6405

Angela R. S. Kruse − Mass Spectrometry Research Center, Vanderbilt University, Nashville, Tennessee 37235, United States; Department of Biochemistry, Vanderbilt University, Nashville, Tennessee 37205, United States; ⓞ orcid.org/0000-0001-8776-2769

Raf Van de Plas − Delft Center for Systems and Control, Delft University of Technology, 2628 CD Delft, The Netherlands; ⓞ orcid.org/0000-0002-2232-7130

Richard M. Caprioli − Department of Chemistry, Vanderbilt University, Nashville, Tennessee 37235, United States; Mass Spectrometry Research Center, Vanderbilt University, Nashville, Tennessee 37235, United States; Department of Biochemistry, Vanderbilt University, Nashville, Tennessee 37205, United States; Department of Pharmacology, Vanderbilt University, Nashville, Tennessee 37232, United States; Department of Medicine, Vanderbilt University, Nashville, Tennessee 37232, United States

Complete contact information is available at:
https://pubs.acs.org/10.1021/acs.analchem.2c03939

Author Contributions

All authors have given approval to the final version of the manuscript.

Notes

The authors declare no competing financial interest.

REFERENCES

(1) Svennerholm, L. J. Lipid Res. 1964, 5, 145−155.
(2) Yu, R. K.; Tsai, Y. T.; Ariga, T.; Yanagisawa, M. J. Oleo Sci. 2011, 60, 537−544.
(3) Sonnino, S.; Mauri, L.; Chigorno, V.; Prinetti, A. Glycobiology 2007, 17, 1R−13R.

(4) Lunghi, G.; Fazzari, M.; Di Biase, E. Di; Mauri, L.; Chiricozzi, E.; Sonnino, S. *FEBS Open Bio.* **2021**, *11*, 3193.

(5) Benady, A.; Freidin, D.; Pick, C. G.; Rubovitch, V. *Sci. Rep.* **2018**, *8*, 1–10.

(6) Kaida, K.; Ariga, T.; Yu, R. K. *Glycobiology* **2009**, *19*, 676–692.

(7) Yuki, N.; Suzuki, K. *Proc. Jpn. Acad. Ser. B Phys. Biol. Sci.* **2012**, *88*, 299–326.

(8) Ariga, T.; McDonald, M. P.; Yu, R. K. *J. Lipid Res.* **2008**, *49*, 1157–1175.

(9) Alpaugh, M.; Galleguillos, D.; Forero, J.; Morales, L. C.; Lackey, S.; Kar, P.; Di Pardo, A.; Holt, A.; Kerr, B. J.; Todd, K. G.; Baker, G. B.; Fouad, K.; Sipione, S. *EMBO Mol. Med.* **2017**, *9*, 1537–1557.

(10) Dufresne, M.; Guneysu, D.; Patterson, N. H.; Marcinkiewicz, M. M.; Regina, A.; Demeule, M.; Chaurand, P. *Anal. Bioanal. Chem.* **2017**, *409*, 1425–1433.

(11) Metelmann, W.; Vukelić, Ž.; Peter-Katalinić, J. *J. Mass Spectrom.* **2001**, *36*, 21–29.

(12) Kotani, M.; Kawashima, I.; Ozawa, H.; Terashima, T.; Tai, T. *Glycobiology* **1993**, *3*, 137–146.

(13) Vajn, K.; Viljetić, B.; Degmečić, I. v.; Schnaar, R. L.; Heffer, M. *PLoS One* **2013**, *8*, No. e75720.

(14) Li, Z.; Zhang, Q. *Anal. Bioanal. Chem.* **2021**, *413*, 3269–3279.

(15) O'connor, P. B.; Mirgorodskaya, E.; Costello, C. E. *J. Am. Soc. Mass Spectrom.* **2002**, *13*, 402–407.

(16) Zhang, Y.; Wang, J.; Liu, J.; Han, J.; Xiong, S.; Yong, W.; Zhao, Z. *Sci. Rep.* **2016**, *6*, 1–11.

(17) Ito, E.; Tominaga, A.; Waki, H.; Miseki, K.; Tomioka, A.; Nakajima, K.; Kakehi, K.; Suzuki, M.; Taniguchi, N.; Suzuki, A. *Neurochem. Res.* **2012**, *37*, 1315–1324.

(18) Caprioli, R. M.; Farmer, T. B.; Gile, J. *Anal. Chem.* **1997**, *69*, 4751–4760.

(19) El-Aneed, A.; Cohen, A.; Banoub, J. *Appl. Spectrosc. Rev.* **2009**, *44*, 210–230.

(20) Weishaupt, N.; Caughlin, S.; Yeung, K. K.-C.; Whitehead, S. N.; Mikula, S.; Elston, G.; Biswavas Misra, B.; Whitehead, S. N.; Weishaupt, N.; Caughlin, S.; K-C Yeung, K. *Front. Neuroanat.* **2015**, *9*, 155.

(21) Caughlin, S.; Park, D. H.; Yeung, K. K.-C.; Cechetto, D. F.; Whitehead, S. N. *J. Visualized Exp.* **2017**, *2017*, 55254.

(22) Yang, E.; Dufresne, M.; Chaurand, P. *Int. J. Mass Spectrom.* **2019**, *437*, 3–9.

(23) Colsch, B.; Jackson, S. N.; Dutta, S.; Woods, A. S. *ACS Chem. Neurosci.* **2011**, *2*, 213–222.

(24) Jackson, S. N.; Ugarov, M.; Egan, T.; Post, J. D.; Langlais, D.; Albert Schultz, J. A.; Woods, A. S. *J. Mass Spectrom.* **2007**, *42*, 1093–1098.

(25) Jackson, S. N.; Benoit, C.; Egan, T.; Lewis, E. K.; Schultz, J. A.; Woods, A. S. *Analyst* **2011**, *136*, 463–466.

(26) Tobias, F.; Pathmasiri, K. C.; Cologna, S. M. *Anal. Bioanal. Chem.* **2019**, *411*, 5659–5668.

(27) Hájek, R.; Jirásko, R.; Lísa, M.; Cífková, E.; Holčapek, M. *Anal. Chem.* **2017**, *89*, 12425–12432.

(28) May, J. C.; Goodwin, C. R.; Lareau, N. M.; Leaptrot, K. L.; Morris, C. B.; Kurulugama, R. T.; Mordehai, A.; Klein, C.; Barry, W.; Darland, E.; Overney, G.; Imatani, K.; Stafford, G. C.; Fjeldsted, J. C.; McLean, J. A. *Anal. Chem.* **2014**, *86*, 2107–2116.

(29) Valentine, S. J.; Koeniger, S. L.; Clemmer, D. E. *Anal. Chem.* **2003**, *75*, 6202–6208.

(30) Zhong, Y.; Hyung, S.-J.; Ruotolo, B. T. *Analyst* **2011**, *136*, 3534.

(31) Shvartsburg, A. A.; Smith, R. D. *Anal. Chem.* **2008**, *80*, 9689–9699.

(32) Deng, L.; Ibrahim, Y. M.; Baker, E. S.; Aly, N. A.; Hamid, A. M.; Zhang, X.; Zheng, X.; Garimella, S. V. B.; Webb, I. K.; Prost, S. A.; Sandoval, J. A.; Norheim, R. V.; Anderson, G. A.; Tolmachev, A. V.; Smith, R. D. *ChemistrySelect* **2016**, *1*, 2396–2399.

(33) Ibrahim, Y. M.; Hamid, A. M.; Deng, L.; Garimella, S. V. B.; Webb, I. K.; Baker, E. S.; Smith, R. D. *Analyst* **2017**, *142*, 1010–1021.

(34) Purves, R. W.; Guevremont, R. *Int. J. Mass Spectrom. Ion Processes* **1999**, *71*, 2346–2357.

(35) Kolakowski, B. M.; Mester, Z. *Analyst* **2007**, *132*, 842.

(36) Guevremont, R. *J. Chromatogr. A* **2004**, *1058*, 3–19.

(37) Fernandez-Lima, F.; Kaplan, D. A.; Suetering, J.; Park, M. A. *Int. J. Ion Mobility Spectrom.* **2011**, *14*, 93.

(38) Michelmann, K.; Silveira, J. A.; Ridgeway, M. E.; Park, M. A. *J. Am. Soc. Mass Spectrom.* **2015**, *26*, 14–24.

(39) Rivera, E. S.; Djambazova, K. v.; Neumann, E. K.; Caprioli, R. M.; Spraggins, J. M. *J. Mass Spectrom.* **2020**, *55*, No. e4614.

(40) Sans, M.; Feider, C. L.; Eberlin, L. S. *Curr. Opin. Chem. Biol.* **2018**, *42*, 138–146.

(41) Sarbu, M.; Robu, A. C.; Ghiulai, R. M.; Vukelić, Ž.; Clemmer, D. E.; Zamfir, A. D. *Anal. Chem.* **2016**, *88*, 5166–5178.

(42) Sarbu, M.; Clemmer, D. E.; Zamfir, A. D. *Biochimie* **2020**, *177*, 226–237.

(43) Sarbu, M.; Petrica, L.; Clemmer, D. E.; Vukelić, Ž.; Zamfir, A. D. *J. Am. Soc. Mass Spectrom.* **2021**, *32*, 1249–1257.

(44) Wormwood Moser, K. L.; Van Aken, G.; DeBord, D.; Hatcher, N. G.; Maxon, L.; Sherman, M.; Yao, L.; Ekroos, K. *Anal. Chim. Acta* **2021**, *1146*, 77–87.

(45) Jackson, S. N.; Muller, L.; Roux, A.; Oktem, B.; Moskovets, E.; Doroshenko, V. M.; Woods, A. S. *J. Am. Soc. Mass Spectrom.* **2018**, *29*, 1463–1472.

(46) Hernandez, D. R.; DeBord, J. D.; Ridgeway, M. E.; Kaplan, D. A.; Park, M. A.; Fernandez-Lima, F. *Analyst* **2014**, *139*, 1913–1921.

(47) Ridgeway, M. E.; Lubeck, M.; Jordens, J.; Mann, M.; Park, M. A. *Int. J. Mass Spectrom.* **2018**, *425*, 22–35.

(48) Silveira, J. A.; Ridgeway, M. E.; Park, M. A. *Anal. Chem.* **2014**, *86*, 5624–5627.

(49) Spraggins, J. M.; Djambazova, K. V.; Rivera, E. S.; Migas, L. G.; Neumann, E. K.; Fuetterer, A.; Suetering, J.; Goedecke, N.; Ly, A.; Van de Plas, R.; Caprioli, R. M. *Anal. Chem.* **2019**, *91*, 14552–14560.

(50) Djambazova, K.; Klein, D. R.; Migas, L. G.; Neumann, E. K.; Rivera, E. S.; Van de Plas, R.; Caprioli, R. M.; Spraggins, J. M. *Anal. Chem.* **2020**, *92*, 13290–13297.

(51) Fu, T.; Oetjen, J.; Chapelle, M.; Verdu, A.; Szesny, M.; Chaumot, A.; Degli-Esposti, D.; Geffard, O.; Clément, Y.; Salvador, A.; Ayciriex, S. *J. Mass Spectrom.* **2020**, *55*, No. e4531.

(52) Chaurand, D. E.; Schwartz, D. A.; Billheimer, D.; Xu, R.; Crecelius, P. E.; Caprioli, B. J.; Caprioli, R. M.; Sanders, M. E.; Jensen, R. A.; Bhattacharya, S. H.; Gal, A. A.; Murray, K. K. *J. Am. Soc. Mass Spectrom.* **2004**, *76*, 1145.

(53) Lein, E. S.; Hawrylycz, M. J.; Ao, N.; Ayres, M.; Bensinger, A.; Bernard, A.; Boe, A. F.; Boguski, M. S.; Brockway, K. S.; Byrnes, E. J.; Chen, L.; Chen, L.; Chen, T.-M.; Chi Chin, M.; Chong, J.; Crook, B. E.; Czaplinska, A.; Dang, C. N.; Datta, S.; Dee, N. R.; Desaki, A. L.; Desta, T.; Diep, E.; Dolbeare, T. A.; Donelan, M. J.; Dong, H.-W.; Dougherty, J. G.; Duncan, B. J.; Ebbert, A. J.; Eichele, G.; Estin, L. K.; Faber, C.; Facer, B. A.; Fields, R.; Fischer, S. R.; Fliss, T. P.; Frensley, C.; Gates, S. N.; Glattfelder, K. J.; Halverson, K. R.; Hart, M. R.; Hohmann, J. G.; Howell, M. P.; Jeung, D. P.; Johnson, R. A.; Karr, P. T.; Kawal, R.; Kidney, J. M.; Knapik, R. H.; Kuan, C. L.; Lake, J. H.; Laramee, A. R.; Larsen, K. D.; Lau, C.; Lemon, T. A.; Liang, A. J.; Liu, Y.; Luong, L. T.; Michaels, J.; Morgan, J. J.; Morgan, R. J.; Mortrud, M. T.; Mosqueda, N. F.; Ng, L. L.; Ng, R.; Orta, G. J.; Overly, C. C.; Pak, T. H.; Parry, S. E.; Pathak, S. D.; Pearson, O. C.; Puchalski, R. B.; Riley, Z. L.; Rockett, H. R.; Rowland, S. A.; Royall, J. J.; Ruiz, M. J.; Sarno, N. R.; Schaffnit, K.; Shapovalova, N. V.; Sivisay, T.; Slaughterbeck, C. R.; Smith, S. C.; Smith, K. A.; Smith, B. I.; Sodt, A. J.; Stewart, N. N.; Stumpf, K.-R.; Sunkin, S. M.; Sutram, M.; Tam, A.; Teemer, C. D.; Thaller, C.; Thompson, C. L.; Varnam, L. R.; Visel, A.; Whitlock, R. M.; Wohnoutka, P. E.; Wolkey, C. K.; Wong, V. Y.; Wood, M.; Yaylaoglu, M. B.; Young, R. C.; Youngstrom, B. L.; Feng Yuan, X.; Zhang, B.; Zwingman, T. A.; Jones, A. R. *Nature* **2006**, *445*, 168–176.

(54) Ng, L.; Bernard, A.; Lau, C.; Overly, C. C.; Dong, H.-W.; Kuan, C.; Pathak, S.; Sunkin, S. M.; Dang, C.; Bohland, J. W.; Bokil, H.;

Mitra, P. P.; Puelles, L.; Hohmann, J.; Anderson, D. J.; Lein, E. S.; Jones, A. R.; Hawrylycz, M. *Nat. Neurosci.* **2009**, *12*, 356−362.

(55) Spraggins, J. M.; Rizzo, D. G.; Moore, J. L.; Rose, K. L.; Hammer, N. D.; Skaar, E. P.; Caprioli, R. M. *J. Am. Soc. Mass Spectrom.* **2015**, *26*, 974−985.

(56) Watson, C.; Paxinos, G.; Kayalioglu, G.; Heise, C. Atlas of the Rat Spinal Cord. In *The Spinal Cord*; Academic Press, 2009; pp 238−306.

(57) Kotani, M.; Kawashima, D.; Ozawa, H.; Terashima, T.; Tai, T. *Glycobiology* **1993**, *3*, 137.

(58) Taki, T. *Biol. Pharm. Bull.* **2012**, *35*, 1642−1647.

(59) Oikawa, N.; Matsubara, T.; Fukuda, R.; Yasumori, H.; Hatsuta, H.; Murayama, S.; Sato, T.; Suzuki, A.; Yanagisawa, K. *PLoS One* **2015**, *10*, No. e0121356.